J Biomol NMR (2009) 45:197–206
DOI 10.1007/s10858-009-9348-5

ARTICLE

Quantitative analysis of backbone motion in proteins using MAS solid-state NMR spectroscopy

Veniamin Chevelkov · Uwe Fink · Bernd Reif

Received: 31 May 2009 / Accepted: 26 June 2009 / Published online: 24 July 2009

Abstract We present a comprehensive analysis of protein dynamics for a micro-crystallin protein in the solid-state. Experimental data include ^{15}N T_1 relaxation times measured at two different magnetic fields as well as ^{1}H–^{15}N dipole, ^{15}N CSA cross correlated relaxation rates which are sensitive to the spectral density function $J(0)$ and are thus a measure of T_2 in the solid-state. In addition, global order parameters are included from a ^{1}H,^{15}N dipolar recoupling experiment. The data are analyzed within the framework of the extended model-free Clore–Lipari–Szabo theory. We find slow motional correlation times in the range of 5 and 150 ns. Assuming a wobbling in a cone motion, the amplitude of motion of the respective amide moiety is on the order of 10° for the half-opening angle of the cone in most of the cases. The experiments are demonstrated using a perdeuterated sample of the chicken α-spectrin SH3 domain.

Keywords MAS solid-state NMR · Protein dynamics · Order parameter · Relaxation · Slow correlated motion · Perdeuterated proteins · Alpha-spectrin SH3

Introduction

Characterization of internal protein dynamics is important to obtain a better understanding of the energetics involved in ligand binding (Frederick et al. 2007; Lange et al. 2008), the enzymatic activity of proteins (Eisenmesser et al. 2002; Henzler-Wildman and Kern 2007), protein folding and unfolding (Grey et al. 2006; Korzhnev et al. 2004; Vallurupalli et al. 2008), and to get insight into the dynamics of ion binding sites in RNA and proteins (Eichmüller and Skrynnikov 2005, 2007; Hoogstraten et al. 2000).

Solution-state NMR relaxation measurements are restricted to the detection of motional time scales faster than the tumbling correlation time τ_R of the protein under investigation (Cavanagh et al. 1996). Motion slower than the overall correlation time is masked as the respective spectral density functions decay rapidly above τ_R. Dynamics on a μs to ms timescale can be probed using $R_{1\rho}$ type sequences. The time domain inbetween (ns–μs) is not easily accessibly and can only be sampled by artificially increasing the overall motional correlation time by extending the size of the molecule (Zhang et al. 2006), or by increasing the viscosity of the solution (Xu et al. 2009; Zeeb et al. 2003), assuming that local dynamics are unaffected. Alternatively, slow motional processes can be identified by comparison of order parameters obtained from ^{15}N relaxation and RDC measurements using multiple alignment media (Bouvignies et al. 2005; Lakomek et al. 2005). RDC measurements will, however, only yield information on the amplitude of the implicated dynamics. The timescale of motion can be accessed only indirectly by exclusion.

On the other hand, analysis of motion comes more and more into the focus of MAS solid-state NMR spectroscopy. In the past, e.g. the loop motion in triosephosphate isomerase was characterized (Williams and McDermott 1995). Analysis of dynamics in the solid-state is even more so of interest as certain parts of the protein are apparently mobile, as the cross-polarization transfer dynamics for

V. Chevelkov · U. Fink · B. Reif (✉)
Leibniz-Forschungsinstitut für Molekulare Pharmakologie (FMP), Robert-Rössle-Str. 10, 13125 Berlin, Germany
e-mail: reif@fmp-berlin.de

B. Reif
Charité Universitätsmedizin, 10115 Berlin, Germany

resonances in mobile regions of the protein can be vanishing (Andronesi et al. 2005; Helmus et al. 2008; Wasmer et al. 2008). In this case, a complete set of resonances can only be employed when scalar transfer sequences are employed (Agarwal and Reif 2008). In contrast to solution-state, overall tumbling is absent in the solid-state. In an immobilized sample, relaxation is exclusively resulting from local structural fluctuations. The dynamic properties of a protein should therefore be accessible with very high accuracy. In particular, motion beyond the overall correlation time limit, imposed in the analysis of dynamics relying on solution-state NMR relaxation data, should be within reach. ^{15}N-T_1 (Chevelkov et al. 2008; Cole and Torchia 1991; Giraud et al. 2004, 2005, 2007), heteronuclear Overhauser effects (Giraud et al. 2006) and ^{15}N-CSA, ^{1}H–^{15}N dipole cross correlated relaxation (Chevelkov et al. 2007a; Skrynnikov 2007) in uniformly isotopically enriched proteins can nowadays be measured routinely on uniformly isotopically enriched proteins. Site-specific order parameters were obtained from dipolar recoupling MAS solid-state NMR experiments for various backbone and sidechain ^{13}C–^{1}H moieties (Franks et al. 2005; Huster et al. 2001; Lorieau and McDermott 2006; Lorieau et al. 2008; Sackewitz et al. 2008). Side chain dynamic information is accessible making use of the deuterium quadrupolar interaction by interpretation of the spinning sideband manifold (Hologne et al. 2005, 2006a, b). ^{2}H/^{13}C-T_1 methyl relaxation measurements allow a more detailed characterization of the motional time scale detected in order parameter experiments (Agarwal et al. 2008; Reif et al. 2006). A comparison of relaxation data obtained in the solid-state and in solution reveals that dynamics in both states is highly similar (Agarwal et al. 2008; Chevelkov et al. 2007c). This opens perspectives for a combined analysis of motion using both solution and solid-state NMR spectroscopy (Palmer-III et al. 1996).

Recently, we suggested a labeling scheme which is based on high levels of deuteration to eliminate most of the undesired proton–proton dipolar interactions (Chevelkov et al. 2006). The perdeuterated protein is recrystallized from a buffer containing 90% D_2O in order to suppress anisotropic interactions among exchangeable sites. Given the fact that high power heteronuclear and homonuclear decoupling is not required, the temperature of the sample is well defined and dynamic properties can be quantified with high accuracy. The deuteration scheme enables a spin-diffusion free determination of dynamic parameters. The goal of the paper is to integrate ^{15}N-T_1, ^{1}H–^{15}N dipole, ^{15}N CSA cross correlated relaxation and ^{1}H–^{15}N dipolar coupling measurements performed in our laboratory to yield a quantitative description of dynamics in the solid-state. The experiments are carried out using a perdeuterated sample of the chicken α-spectrin SH3 domain (Fig. 1).

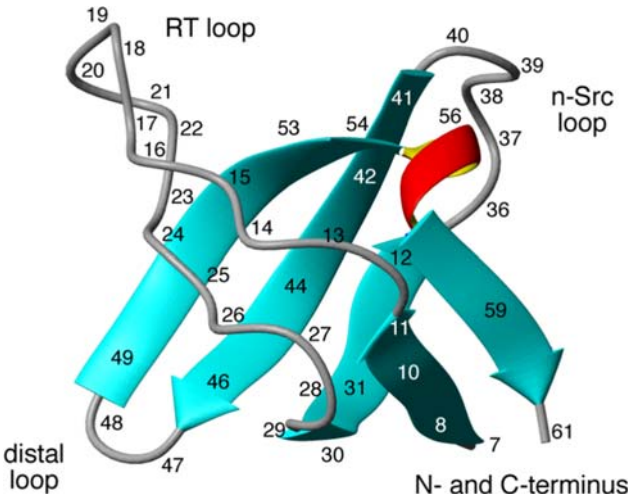

Fig. 1 Structural representation of the α-spectrin SH3 domain (PDB: 1U06; Chevelkov et al. 2005). The nomenclature for the loops are adapted from Serrano and co-worker (Martinez et al. 1998)

Materials and methods

Sample preparation

A pET3d derivative coding for α-spectrin SH3 domain from chicken brain was a gift of M. Saraste. Protein was expressed in *E. coli* BL21 (DE3) in M9 minimal medium with 100% D_2O with 4 g/L $^{2}H_8$-glycerol as the sole carbon source, together with 1 g/L ^{15}N–NH_4Cl. Cells were grown at 37°C up to an optical density ($OD_{600\ nm}$) of 0.6. The temperature was then decreased to 22°C and induction was started with 1 mM IPTG overnight. Purification of the cell extract was carried out in H_2O (anion exchange on a Q-Sepharose FF column, followed by gel filtration on a Superdex75 column; Pauli et al. 2000). 10 mg of the purified protein was lyophilized and redissolved in H_2O/D_2O using a mixing ratio of 10:90 with respect to solvent exchangeable protons. Microcrystalline precipitates were obtained by mixing the protein solution (10 mg/mL) at a ratio of 1:1 (v/v) with a 200 mM $(NH_4)_2SO_4$ solution containing 90% D_2O. The pH value was adjusted to around seven by exposing the sample to an alkaline atmosphere, monitoring the pH with pH sensitive paper strips.

NMR spectroscopy

Measurements of the ^{15}N-T_1 relaxation time (Chevelkov et al. 2008), the ^{1}H–^{15}N dipole, ^{15}N CSA cross correlated relaxation rate $\eta^{DD/CSA}$ (Chevelkov et al. 2007a, b; Chevelkov and Reif 2008) and ^{1}H–^{15}N dipolar recoupling experiments (Chevelkov et al. 2009) were carried out as described previously. In particular, ^{1}H detection in combination with perdeuteration was employed to achieve high

sensitivity and resolution (Chevelkov et al. 2003; Reif et al. 2001; Reif and Griffin 2003). All experiments are carried out at an effective sample temperature of 11°C, using a per-deuterated, ^{15}N labeled sample of the α-spectrin SH3 which was recrystallized using a mixture of 10% H_2O and 90% D_2O in the crystallization buffer, as described in (Chevelkov et al. 2006). The assignment of the resonances was obtained using HNCACB type experiments (Linser et al. 2008).

Theoretical background

The analysis of motion in the solid-state is carried out in the framework of Redfield (1957) theory. This approach seems to be valid as we are only considering motional time scales which are faster compared to the size of the involved anisotropic interactions.

The experiment employed to measure ^{15}N T_1 is described in detail in reference (Chevelkov et al. 2008). The measured relaxation rate $R_1(^{15}\mathrm{N})$ is related to the size of the N–H dipolar coupling d, the chemical shift anisotropy c and the spectral densitiy function $J(\omega)$ according to (Cavanagh et al. 1996; Torchia and Szabo 1982)

$$R_1(^{15}\mathrm{N}) = \frac{d^2}{10}[J_0(\omega_\mathrm{H}-\omega_\mathrm{N}) + 3J_1(\omega_\mathrm{N}) + 6J_2(\omega_\mathrm{H}+\omega_\mathrm{N})] + \frac{2}{15}c^2 J_1(\omega_\mathrm{N}) \quad (1)$$

with

$$d^2 = \left(\frac{\gamma_\mathrm{H}\gamma_\mathrm{N}h}{2\pi r_\mathrm{NH}^3}\right)^2 \equiv \omega_\mathrm{HN}^2$$
$$c^2 = [\gamma_\mathrm{N}B_0(\sigma_\parallel - \sigma_\perp)]^2 \equiv \omega_\mathrm{N}^2 \times \Delta\sigma^2 \quad (2)$$

and r_NH refers to the ^{1}H–^{15}N bond length. ω_H and ω_N represent the ^{1}H and the ^{15}N Larmor frequencies, respectively. The frequency of the ^{1}H,^{15}N dipole–dipole interaction is denoted as ω_HN. The ^{15}N CSA can be assumed to be axially symmetric. The ^{15}N–^{1}H bond is tilted by $\sim 20°$ with respect to the principal axis of the ^{15}N CSA tensor (Chekmenev et al. 2004). Typical values for the anisotropy of the ^{15}N chemical shift are $\Delta\sigma = \sigma_\parallel - \sigma_\perp = 170 \pm 8$ ppm, or $\sigma_z = 106 \pm 6$ ppm (Chekmenev et al. 2004; Franks et al. 2005; Hall and Fushman 2006; Wylie et al. 2006, 2007). In the absence of motion, an effective N–H bond length of $r_\mathrm{NH} = (\langle r_\mathrm{NH}^3\rangle)^{1/3} = 1.015$ Å is assumed (Yao et al. 2008).

In the solid-state, the exact form of the spectral density function depends on the underlying motional model (Torchia and Szabo 1982). In the framework of the extended model free formalism (Clore et al. 1990; Lipari and Szabo 1982), the spectral density functions $J_\mathrm{m}(\omega)$ are expressed as lorentzian functions depending on two correlation times τ_s and τ_F, and two order parameters S_S and S_F, respectively, referring to slow and fast motional processes

$$J(\omega) = (1-S_F^2)\frac{\tau_F}{1+\omega^2\tau_F^2} + S_F^2(1-S_S^2)\frac{\tau_S}{1+\omega^2\tau_S^2} \quad (3)$$

In order to obtain a "T_2 type" observable which depends on $J(0)$, ^{1}H–^{15}N dipole, ^{15}N CSA cross correlated relaxation rates $\eta^{\mathrm{DD/CSA}}$ were measured. Quantitative values for $\eta^{\mathrm{DD/CSA}}$ were extracted from a constant-time experiment in which protons are not decoupled in the indirect evolution period (Chevelkov et al. 2007a). The integral intensity ratio of the N–H^α/N–H^β multiplet components after a relaxation delay is directly related to the cross correlated relaxation rates $\eta^{\mathrm{DD/CSA}}$. In the solid-state, the Hamiltonian describing an isolated ^{1}H,^{15}N spin pair is inhomogeneous in the sense of Maricq and Waugh (Maricq and Waugh 1979). If the spinning rate is larger than the size of the CSA and dipole-dipole interaction, the ^{15}N line width is only determined by motional processes. However, even at a MAS rotation frequency of 24 kHz coherent effects are not completely averaged out (Chevelkov et al. 2007b). In a spin system, in which the proton of the ^{1}H,^{15}N pair is integrated into a proton spin network, the Hamiltonian is no longer inhomogeneous. Similar arguments apply for protonated samples in the limit of insufficient ^{1}H decoupling. The decay of ^{15}N transverse magnetization is therefore not only due to relaxation, but influenced as well by the proton spin bath. In this system, the ^{15}N T_2 relaxation can not be used directly to probe motional properties of the protein. Even in the heavily proton dilute protein sample used in this study, the proton line width depends still weakly on the MAS frequency (Chevelkov et al. 2006), reflecting residual long range proton interactions. Simulations in which three additional protons are taken into account (assuming mutual ^{1}H, ^{1}H dipolar interactions on the order of 800–1,200 Hz) yield a uniform increase in the line width of both the H^α and H^β multiplet component of the ^{15}N spectrum (Chevelkov et al. 2007a). Our experimental approach is supported by numerical simulations in which coherent and incoherent cross correlation effects are explicitly coded under magic angle spinning (Skrynnikov 2007). Incoherent effects like cross correlated relaxation result in a differential line width of the N–H^α/N–H^β multiplet components. Coherent effects like static correlations between the dipolar and the CSA interaction will at the same time not affect the relative N–H^α/N–H^β resonance line width.

The cross correlated relaxation rate $\eta^{\mathrm{DD/CSA}}$ can be described again as a function of spectral density functions, using the equation (Fushman and Cowburn 1998; Tjandra et al. 1996)

$$\eta^{\mathrm{DD/CSA}} = \frac{\mathrm{d}c}{15}\{4J_0(0) + 3J_1(\omega_{\mathrm{N}})\}P_2(\cos\theta) \quad (4)$$

where $P_2(x) = (3x^2 - 1)/2$ corresponds to the second order Legendre polynomial, θ represents the angle between the principal axis of the ^{15}N–^{1}H dipolar vector and the ^{15}N CSA shielding tensor, and adopts values on the order of ca. 20°.

The last input parameter employed in the fitting analysis is the generalized order parameter $S = S_S S_F$. In solid-state NMR, S refers to the ratio of the motionally averaged dipolar coupling to its value in the static limit. The generalized order parameter S for each amide moiety is therefore implicitly contained in the size of the individual experimental N–H dipolar coupling. To quantitatively access the dipolar couplings, we made use of a phase-inverted CP (CPPI) experiment which is insensitive to RF inhomogeneity and thus yields the absolute dipolar coupling with high accuracy (Dvinskikh et al. 2003, 2005; Wu and Zilm 1993). We have shown that fluctuations of the N–H bond length due to differential hydrogen bonding are within the experimental error of the estimation of the size of the coupling and can therefore be neglected in the analysis (Chevelkov et al. 2009). In case the motional model implies a wobbling of the N–H bond vector within a cone with an half-opening angle α_0, the general order parameter S can be expressed as (Lipari and Szabo 1981; Palmer-III et al. 1996)

$$\langle S \rangle = \frac{1}{2}\langle 3\cos^2\alpha - 1 \rangle = \frac{1}{2}(1 + \cos\alpha_0)\cos\alpha_0 \quad (5)$$

In this model, an half-opening angle of $\alpha = 21°$ yields an general order parameter $S = 0.9$.

Results and discussion

In the following, we combine all experimental results ($^{15}R_1$ measured at an external field of 14.1 T and 21.1 T, corresponding to ^{1}H Larmor frequency of 600 MHz and 900 MHz; ^{1}H–^{15}N dipole, ^{15}N CSA cross correlated relaxation rate $\eta^{\mathrm{DD/CSA}}$ and ^{1}H,^{15}N dipolar couplings) in a multi-dimensional grid search to find the best fit conditions

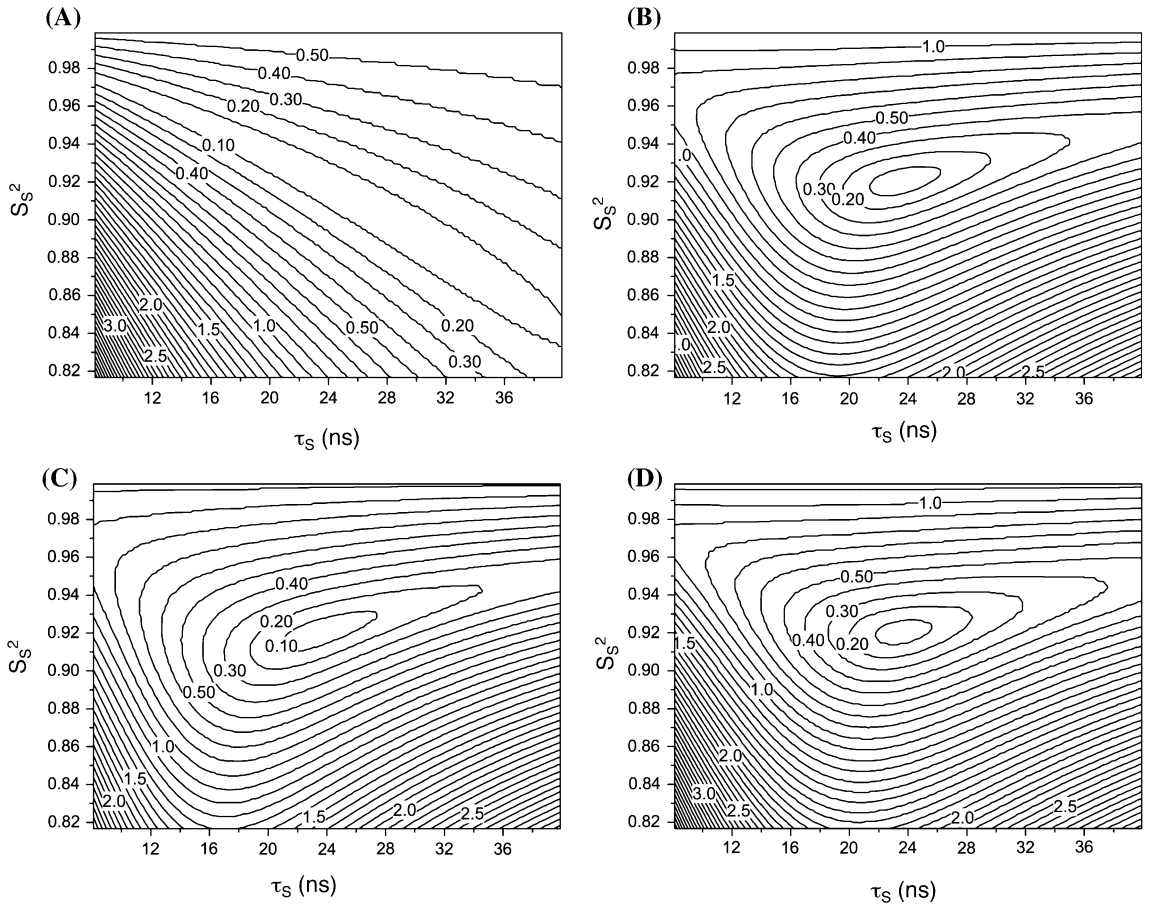

Fig. 2 Rms difference plots between experimental and theoretical data as a function of S_S^2 and τ_S for the residue Q16 in α-spectrin SH3. For the best fit, we obtain $\tau_F = 22$ ps, and $S_F^2 = 0.819$. Data included in the fit are: **a** ^{15}N T_1 measured at 14.1 T and 21.1 T. **b** ^{15}N T_1 measured at 14.1 T and $\eta^{\mathrm{DD/CSA}}$. **c** ^{15}N T_1 measured at 21.1 T $+\eta^{\mathrm{DD/CSA}}$. **d** ^{15}N T_1 measured at 14.1 T, ^{15}N T_1 measured at 21.1 T and $\eta^{\mathrm{DD/CSA}}$

in the framework of an extended model-free analysis (Clore et al. 1990; Lipari and Szabo 1982). In total, the data contains four experimental observables. The extended model-free spectral densities are dependent on four parameters, in particular, the slow and fast motional correlation times τ_s and τ_F, and the order parameters for slow and fast motion S_S and S_F, respectively. Obviously, the data are rather sparse. Therefore, the results obtained for each amide need to be evaluated to rationalize if the data and the employed model allow a consistent description of the system. The root mean square deviation χ between experimental and theoretical rates is defined as

$$\chi^2 = \left\{ \sum_i \left[\frac{1}{R_{1,i}^{\text{expt}}} \left(R_{1,i}^{\text{theo}} - R_{1,i}^{\text{expt}} \right) \right]^2 + \left[\frac{1}{\eta^{\text{expt}}} (\eta^{\text{theo}} - \eta^{\text{expt}}) \right]^2 \right\} \tag{6}$$

Superscripts theo and expt denote the theoretical and experimental values for the ^{15}N longitudinal relaxation rate R_1 and the ^{1}H–^{15}N dipole, ^{15}N CSA cross-correlated relaxation rate $\eta^{\text{DD/CSA}}$. The theoretical values for the relaxation rates were calculated using Eqs. 1–4. In all calculations, the dipolar coupling derived general order parameter is employed. A 3D grid search was performed allowing the parameters times τ_S, τ_F and S_S^2 to float freely, while the order parameter of fast motion S_F^2 was calculated according to $S_F = S/S_S$.

Figure 2 shows RMSD contour plots for residue Q16 of the α-spectrin SH3 domain as a function of τ_S and S_S^2. τ_F was set to 22 ps, which corresponds to its optimal value obtained in the course of the grid search. Whereas in the fitting underlying Fig. 2a only ^{15}N-T_1 are included, Fig. 2b–d contain as well cross-correlated relaxation data ($\eta^{\text{DD/CSA}}$). We find that the minimum for the fit of the motional correlation time τ_S is more restricted if $\eta^{\text{DD/CSA}}$ is taken into account. Inclusion of an additional ^{15}N-T_1 relaxation time measured at a different external field strength increases the steepness of the minimum, but leaves the best fit for τ_S and S_S^2 approximately unaltered. This is in agreement with previous findings (Chevelkov et al. 2007c; Giraud et al. 2005).

In the following, we represent the various best fit values as a function of the protein sequence. Figure 3 shows the overall order parameter as well as the order parameter for slow motional processes, together with the implicated half-opening angle, for the α-spectrin SH3 domain. The general order parameter $<S>$ was set to 1 assuming an effective N–H bond length of $r_{\text{eff}} = (<r_{\text{NH}}^{-3}>)^{-1/3} = 1.015$ Å (Yao et al. 2008). We find in general lower order parameters at

Fig. 4 Slow and fast motional correlation times τ_S and τ_F as a function of the primary sequence in α-spectrin SH3. *Black squares* refer to the best fit value for τ_S and τ_F, respectively. *Red circles* and *green triangles* denote the result of the RMSD fitting obtained by changing the experimental ^{15}N-T_1 relaxation time obtained at 14.1 T (**a**, **b**), the measured ^{1}H–^{15}N, ^{15}N-CSA cross correlated relaxation rate $\eta^{\text{DD/CSA}}$ (**c**, **d**) and the overall motional parameter $1 - <S>$ (**e**, **f**) by +/– 10%, respectively. The *panels* at the *bottom* of each figure show the results obtained for Y13, R21, D40 and L8, V46, R49, D62, respectively, for which we find particularly long values for τ_S. For residues L8, V46, R49 and D62, τ_F becomes exceptionally long, indicating that motion is more complicated, and that the extended model free analysis is no longer sufficient to describe the motional process

Fig. 3 Order parameter S^2 as a function of the primary sequence in α-spectrin SH3. *Black squares* denote the order parameter of slow motional processes, whereas *red circles* indicate the overall order parameter $S_S^2 S_F^2$. The vertical axis on the right hand side of the figure displays the half-opening angle α_0 assuming a "wobbling in a cone" motion, making use of Eq. 5

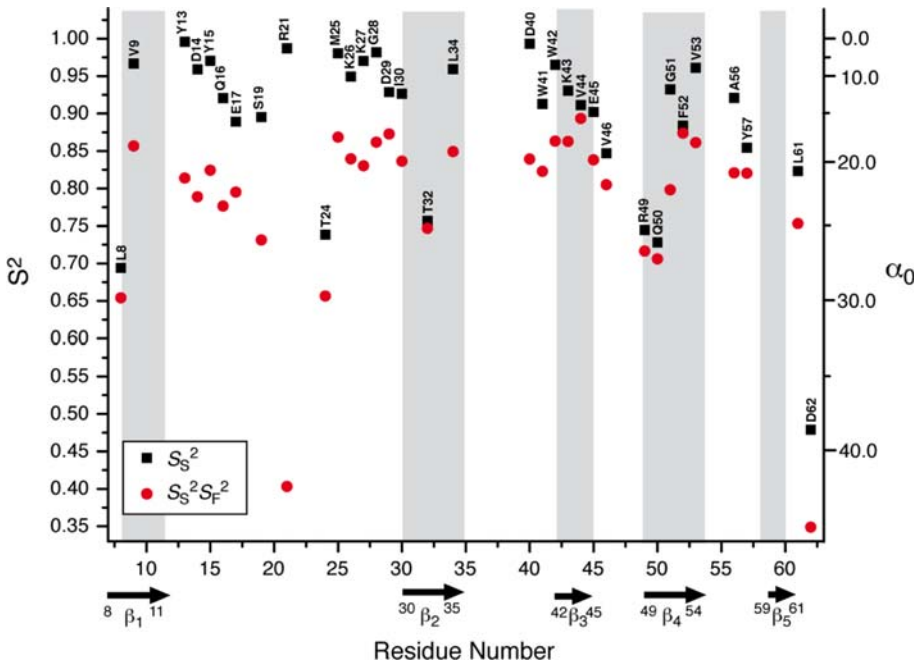

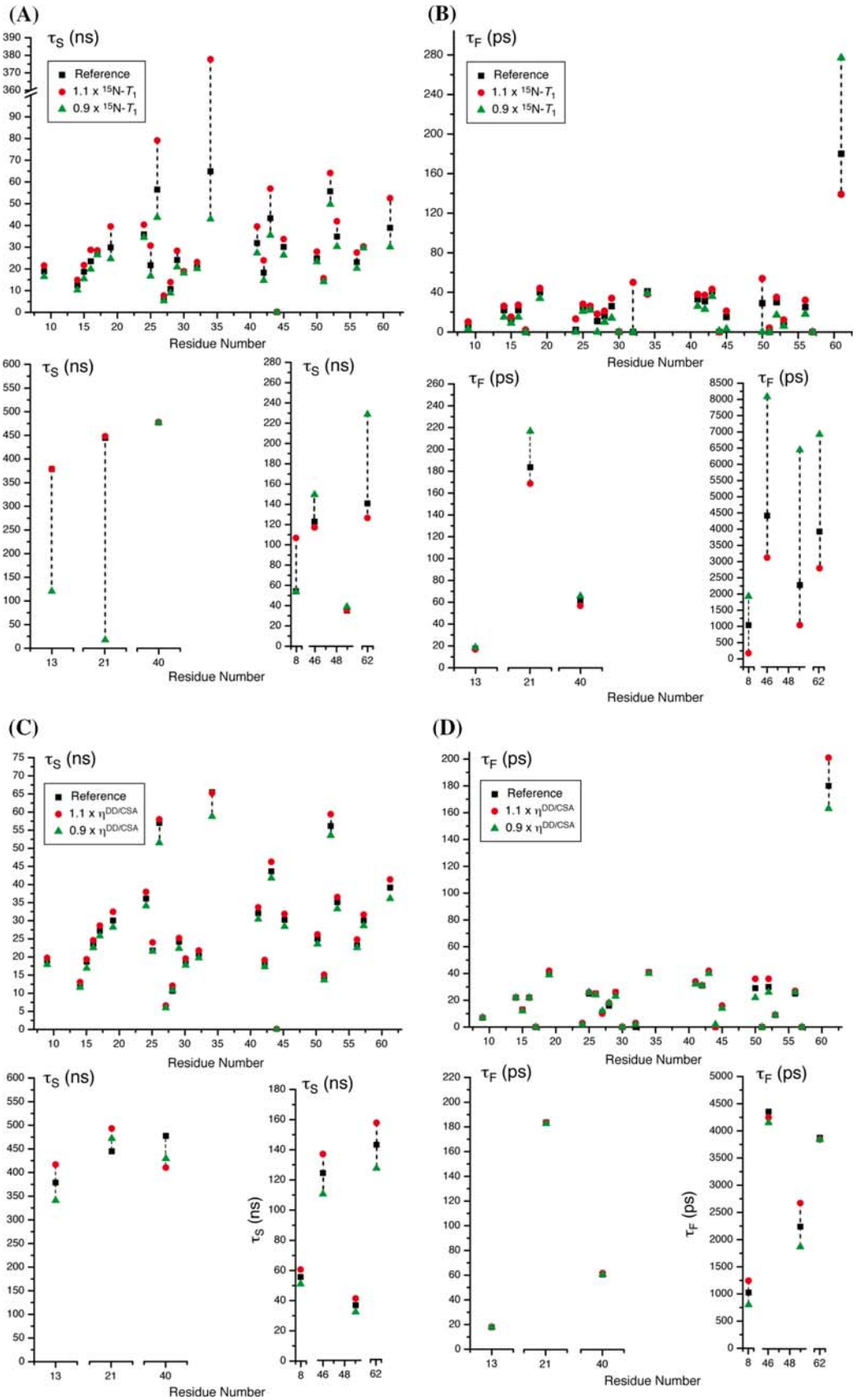
(A)
τS (ns)
Reference
1.1 x 15N-T1
0.9 x 15N-T1
Residue Number
(B)
τF (ps)
Reference
1.1 x 15N-T1
0.9 x 15N-T1
Residue Number
(C)
τS (ns)
Reference
1.1 x ηDD/CSA
0.9 x ηDD/CSA
Residue Number
(D)
τF (ps)
Reference
1.1 x ηDD/CSA
0.9 x ηDD/CSA
Residue Number

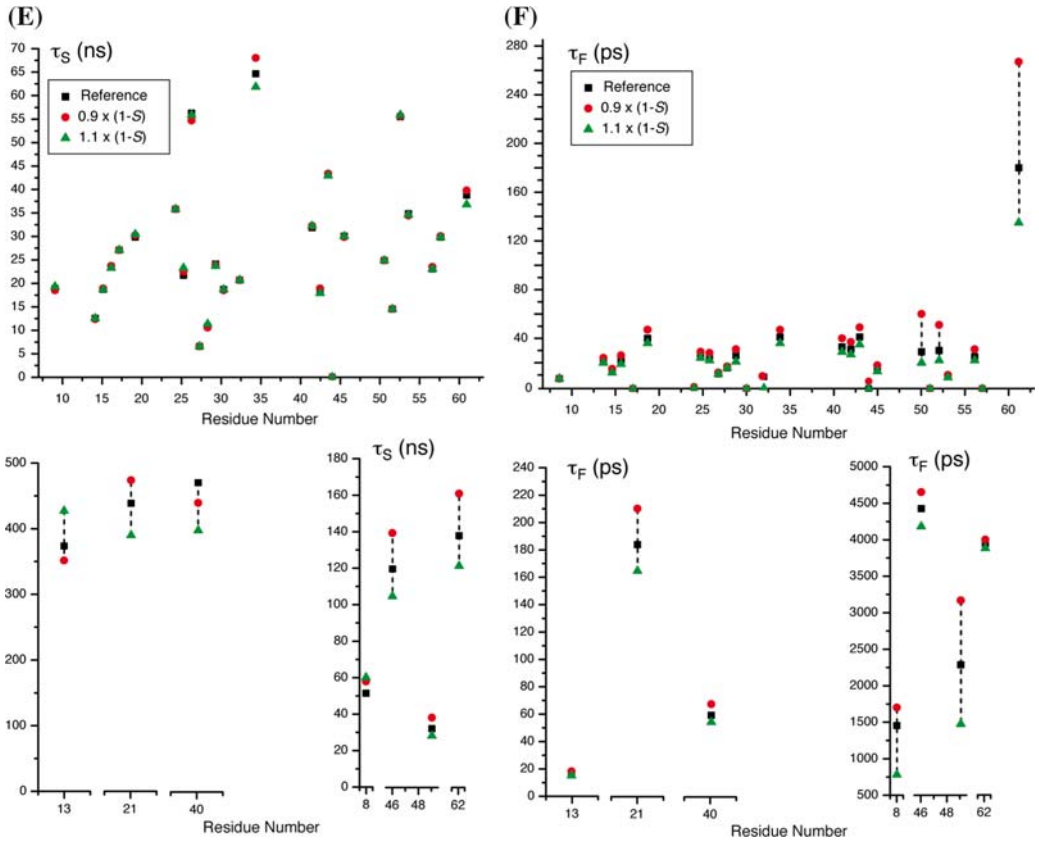

Fig. 4 continued

the N- and C-terminus. The average order parameter for slow motional processes in on the order of $S_S^2 = 0.95$, corresponding to an half-opening angle of ca. 10° assuming a diffusion in a cone motion (Lipari and Szabo 1981).

The correlation times of slow and fast motion τ_S and τ_F are shown in Fig. 4. Black squares represent the best fit values. Red circles and green triangles denote the result of the RMSD fitting obtained by changing the experimental ^{15}N-T_1 relaxation time (a, b), the measured ^{1}H–^{15}N, ^{15}N-CSA cross correlated relaxation rate $\eta^{DD/CSA}$ (c, d) and the overall motional parameter $1 - \langle S \rangle$ (e, f) by ± 10%, respectively. Residues displayed at the bottom of Fig. 4 show unusual large values and are therefore plotted separately. Non-canonical residues are L8, Y13, R21, D40, V46, R49 and D62. For residues Y13, R21 and D40, we find very high slow motional order parameters S_S^2 which are on the order of 0.9959, 0.9871 and 0.9932, respectively. Motion for those residues seems considerably restricted. The high value for S_S^2 implies that only fast motional processes contribute to the spectral density (2). For canonical residues, the slow motional correlation time τ_S varies between 5 and 70 ns. The second set of non-canonical residues comprises residues L8, V46, R49 and D62. For those residues, τ_F fits to values on the order of several nanoseconds and τ_S can be as large as 150 ns. For these residues, we find high values of $\eta^{DD/CSA}$ on the order of 10 Hz, or larger. Residue V46 is located in the distal loop. The adjecent residues N47 and D48 have strongly increased B-factors in the X-ray structure and are not observed in solid-state NMR spectra. It is therefore plausible that V46 is undergoing slow dynamics. This is supported by the exceptionally long value for τ_F (4.5 ns) for V46 and R49. For these residues, the extended model-free analysis might represent an over-simplification. One more motional mode seems to be required in order to describe appropriately the underlying dynamics for these residues, as one would expect a vibrational mode as the fastest dynamic process. Fitting the data using a simple Lipari–Szabo analysis with only two unknown parameters, namely one correlation time τ and one order parameter S^2, reproduces the slow motional correlation time in general rather well (data not shown). We therefore believe that the indicated values for τ_S for the amide moieties of V46 and R49 correctly describe this parameter. A similar explanation applies to L8 and D62 which are located at the N- and C-terminus of the protein and which are virtually the first and last residue for which an electron density can be assigned. D40 is contained in the n-Scr loop. It is noteworthy that the fitting analysis cannot be carried out for residues S36, T37, N38 and K39, as these residues yield significantly reduced

intensities in ^{1}H,^{15}N correlation spectra. The achieveable signal-to-noise ratio for those residues is insufficient to allow a quantitative extraction of any of the described relaxation rates. The reduced intensity might be indicative for very slow motion or a chemical exchange process on a μs–ms time scale. In general, we find τ_F to be on the order of 5–50 ps which would be expected for vibrational dynamics. This is in agreement with the results obtained by Mack et al. (2000) who used field dependent bulk ^{2}H T_1 relaxation times and quadrupolar order parameters of exchangeable deuterons in RNase H to quantify backbone motion. Variations in the experimental ^{15}N-T_1 relaxation time imposes the largest error on the extracted motional correlation times τ_S and τ_F. The fitting procedure breaks down and yields a very larger error, in case the artificially increased ^{15}N-T_1 relaxation time at 14.1 T (red circles in Fig. 4) becomes close to, or larger than the experimental ^{15}N-T_1 relaxation time measured at 21.1 T. Variations in the cross correlated relaxation rate $\eta^{DD/CSA}$ and ^{1}H–^{15}N order parameters produce smaller variations in the extracted slow and fast motional correlation time τ_S and τ_F (Fig. 4c–f).

So far, we are not able to detect long range correlated dynamics which was suggested by the alternating pattern which we observed previously in the ^{15}N-T_1 relaxation times in β-sheet β_2 comprising residues 30–35 (Chevelkov et al. 2008). Long range collective motion was suggested recently for ubiquitin (Lakomek et al. 2005) and protein G (Bouvignies et al. 2005). At this point, we cannot pursue this question in greater detail as the data—in particular in this part of the protein—is still rather sparse. In total, we were able to analyze 34 out of 53 possible amide moieties. Work is going on in our laboratory to obtain a more complete set of data.

Conclusion

In conclusion, we have shown that the dynamic properties of the protein backbone can be characterized in the solid-state with high accuracy, using ^{15}N-T_1 relaxation times measured at two different fields, ^{1}H–^{15}N, ^{15}N-CSA cross correlated relaxation rate $\eta^{DD/CSA}$ and ^{1}H–^{15}N dipolar coupling measurements to obtain overall order parameters. Using the micro-crystalline α-spectrin SH3 domain as a model system, we find slow motional correlation times between 5 and 150 ns. Assuming a wobbling in a cone motion, the amplitude of motion of the respective amide moiety is on the order of 10° for the half-opening angle of the cone in most of the cases. We expect that these experiments will find widespread application in the characterization of dynamic processes of biomolecules such as membrane proteins and amyloidogenic peptides and proteins.

Acknowledgments We thank Nikolai Skrynnikov for many stimulating discussions. This work was supported by the Leibniz-Gemeinschaft and the DFG (grants Re1435, SFB 449, SFB 740).

References

Agarwal V, Reif B (2008) Residual methyl protonation in perdeuterated proteins for multidimensional correlation experiments in MAS solid-state NMR spectroscopy. J Magn Reson 194:16–24

Agarwal V, Xue Y, Skrynnikov NR, Reif B (2008) Protein side-chain dynamics as observed by solution- and solid-state NMR: a similarity revealed. J Am Chem Soc 130:16611–16621

Andronesi OC, Becker S, Seidel K, Heise H, Young HS, Baldus M (2005) Determination of membrane protein structure and dynamics by magic-angle-spinning solid-state NMR spectroscopy. J Am Chem Soc 127:12965–12974

Bouvignies G, Bernado P, Meier S, Cho K, Grzesiek S, Bruschweiler R, Blackledge M (2005) Identification of slow correlated motions in proteins using residual dipolar and hydrogen-bond scalar couplings. Proc Natl Acad Sci USA 102:13885–13890

Cavanagh J, Fairbrother WJ, Palmer AG, Skelton NJ (1996) Protein NMR spectroscopy: principles and practice. Academic Press, San Diego

Chekmenev EY, Zhang Q, Waddell KW, Mashuta MS, Wittebort RJ (2004) ^{15}N chemical shielding in glycyl tripeptides: measurement by solid-state NMR and correlation with X-ray structure. J Am Chem Soc 126:379–384

Chevelkov V, Reif B (2008) TROSY effects in MAS solid-state NMR. Concepts NMR 32A:143–156

Chevelkov V, van Rossum BJ, Castellani F, Rehbein K, Diehl A, Hohwy M, Steuernagel S, Engelke F, Oschkinat H, Reif B (2003) ^{1}H detection in MAS solid state NMR spectroscopy employing pulsed field gradients for residual solvent suppression. J Am Chem Soc 125:7788–7789

Chevelkov V, Faelber K, Diehl A, Heinemann U, Oschkinat H, Reif B (2005) Detection of dynamic water molecules in a microcrystalline sample of the SH3 domain of alpha-spectrin by MAS solid-state NMR. J Biomol NMR 31:295–310

Chevelkov V, Rehbein K, Diehl A, Reif B (2006) Ultra-high resolution in proton solid-state NMR at high levels of deuteration. Angew Chem Int Ed 45:3878–3881

Chevelkov V, Diehl A, Reif B (2007a) Quantitative measurement of differential ^{15}N-Hα/β T2 relaxation times in a perdeuterated protein by MAS solid-state NMR spectroscopy. Magn Res Chem 45:S156–S160

Chevelkov V, Faelber K, Schrey A, Rehbein K, Diehl A, Reif B (2007b) Differential line broadening in MAS solid-state NMR due to dynamic interference. J Am Chem Soc 129:10195–10200

Chevelkov V, Zhuravleva AV, Xue Y, Reif B, Skrynnikov NR (2007c) Combined analysis of ^{15}N relaxation data from solid- and solution-state NMR spectroscopy. J Am Chem Soc 129:12594–12595

Chevelkov V, Diehl A, Reif B (2008) Measurement of ^{15}N–T_1 relaxation rates in a perdeuterated protein by MAS solid-state NMR spectroscopy. J Chem Phys 128:052316

Chevelkov V, Fink U, Reif B (2009) Accurate determination of order parameters from ^{1}H,^{15}N dipolar couplings in MAS solid-state NMR experiments. J Am Chem Soc (submitted)

Clore GM, Szabo A, Bax A, Kay LE, Driscoll PC, Gronenborn AM (1990) Deviations from the Simple 2-parameter model-free

approach to the interpretation of N-15 nuclear magnetic relaxation of proteins. J Am Chem Soc 112:4989–4991
Cole HBR, Torchia DA (1991) An NMR-study of the backbone dynamics of Staphylococcal nuclease in the crystalline state. Chem Phys 158:271–281
Dvinskikh SV, Zimmermann H, Maliniak A, Sandstrom D (2003) Heteronuclear dipolar recoupling in liquid crystals and solids by PISEMA-type pulse sequences. J Magn Reson 164:165–170
Dvinskikh SV, Zimmermann H, Maliniak A, Sandström D (2005) Heteronuclear dipolar recoupling in solid-state nuclear magnetic resonance by amplitude-, phase-, and frequency-modulated Lee–Goldburg cross-polarization. J Chem Phys 122:044512
Eichmüller C, Skrynnikov NR (2005) A new amide proton R-1 rho experiment permits accurate characterization of microsecond time-scale conformational exchange. J Biomol NMR 32:281–293
Eichmüller C, Skrynnikov NR (2007) Observation of mu s time-scale protein dynamics in the presence of Ln(3+)stop ions: application to the N-terminal domain of cardiac troponin C. J Biomol NMR 37:79–95
Eisenmesser EZ, Bosco DA, Akke M, Kern D (2002) Enzyme dynamics during catalysis. Science 295:1520–1523
Franks WT, Zhou DH, Wylie BJ, Money BG, Graesser DT, Frericks HL, Gurmukh S, Rienstra CM (2005) Magic-angle spinning solid-state NMR spectroscopy of the beta 1 immunoglobulin binding domain of protein G (GB1): ^{15}N and ^{13}C chemical shift assignments and conformational analysis. J Am Chem Soc 127:12291–12305
Frederick KK, Marlow MS, Valentine KG, Wand AJ (2007) Conformational entropy in molecular recognition by proteins. Nature 448:325–330
Fushman D, Cowburn D (1998) Model-independent analysis of ^{15}N chemical shift anisotropy from NMR relaxation data. Ubiquitin as a test example. J Am Chem Soc 120:7109–7110
Giraud N, Böckmann A, Lesage A, Penin F, Blackledge M, Emsley L (2004) Site-specific backbone dynamics from a crystalline protein by solid-state NMR spectroscopy. J Am Chem Soc 126:11422–11423
Giraud N, Blackledge M, Goldman M, Böckmann A, Lesage A, Penin F, Emsley L (2005) Quantitative analysis of backbone dynamics in a crystalline protein from nitrogen-15 spin-lattice relaxation. J Am Chem Soc 127:18190–18201
Giraud N, Sein J, Pintacuda G, Böckmann A, Lesage A, Blackledge M, Emsley L (2006) Observation of heteronuclear overhauser effects confirms the ^{15}N–^{1}H dipolar relaxation mechanism in a crystalline protein. J Am Chem Soc 128:12398–12399
Giraud N, Blackledge M, Böckmann A, Emsley L (2007) The influence of nitrogen-15 proton-driven spin diffusion on the measurement of nitrogen-15 longitudinal relaxation times. J Magn Reson 184:51–61
Grey MJ, Tang YF, Alexov E, McKnight CJ, Raleigh DP, Palmer AG (2006) Characterizing a partially folded intermediate of the villin headpiece domain under non-denaturing conditions: contribution of His41 to the pH-dependent stability of the N-terminal subdomain. J Mol Biol 355:1078–1094
Hall JB, Fushman D (2006) Variability of the N-15 chemical shielding tensors in the B3 domain of protein G from N-15 relaxation measurements at several fields. Implications for backbone order parameters. J Am Chem Soc 128:7855–7870
Helmus JJ, Surewicz K, Nadaud PS, Surewicz WK, Jaroniec CP (2008) Molecular conformation and dynamics of the Y145Stop variant of human prion protein in amyloid fibrils. Proc Natl Acad Sci USA 105:6284–6289
Henzler-Wildman K, Kern D (2007) Dynamic personalities of proteins. Nature 450:964–972
Hologne M, Faelber K, Diehl A, Reif B (2005) Characterization of dynamics of perdeuterated proteins by MAS solid-state NMR. J Am Chem Soc 127:11208–11209
Hologne M, Chen Z, Reif B (2006a) Characterization of dynamic processes using deuterium in uniformly ^{2}H, ^{13}C, ^{15}N enriched peptides by MAS solid-state NMR. J Magn Res 179:20–28
Hologne M, Chevelkov V, Reif B (2006b) Deuteration of peptides and proteins in MAS solid-state NMR. Prog NMR Spect 48:211–232
Hoogstraten CG, Wank JR, Pardi A (2000) Active site dynamics in the lead-dependent ribozyme. Biochemistry 39:9951–9958
Huster D, Xiao LS, Hong M (2001) Solid-state NMR investigation of the dynamics of the soluble and membrane-bound colicin Ia channel-forming domain. Biochemistry 40:7662–7674
Korzhnev DM, Salvatella X, Vendruscolo M, Di Nardo AA, Davidson AR, Dobson CM, Kay LE (2004) Low-populated folding intermediates of Fyn SH3 characterized by relaxation dispersion NMR. Nature 430:586–590
Lakomek NA, Fares C, Becker S, Carlomagno T, Meiler J, Griesinger C (2005) Side-chain orientation and hydrogen-bonding imprint supra-tauc motion on the protein backbone of ubiquitin. Angew Chem Int Ed 117:7954–7956
Lange OF, Lakomek N-A, Fares C, Schroeder GF, Walter KFA, Becker S, Meiler J, Grubmueller H, Griesinger C, de Groot BL (2008) Recognition dynamics up to microseconds revealed from an RDC-derived ubiquitin ensemble in solution. Science 320:1471–1475
Linser R, Fink U, Reif B (2008) Proton-detected scalar coupling based assignment strategies in MAS solid-state NMR spectroscopy applied to perdeuterated proteins. J Magn Reson 193:89–93
Lipari G, Szabo A (1981) Pade approximants to correlation-functions for restricted rotational diffusion. J Chem Phys 75:2971–2976
Lipari G, Szabo A (1982) Model-free approach to the interpretation of nuclear magnetic resonance relaxation in macromolecules. 1. Theory and range of validity. J Am Chem Soc 104:4546–4559
Lorieau JL, McDermott AE (2006) Conformational flexibility of a microcrystalline globular protein: order parameters by solid-state NMR spectroscopy. J Am Chem Soc 128:11505–11512
Lorieau JL, Day LA, McDermott AE (2008) Conformational dynamics of an intact virus: order parameters for the coat protein of Pf1 bacteriophage. Proc Natl Acad Sci USA 105:10366–10371
Mack JW, Usha MG, Long J, Griffin RG, Wittebort RJ (2000) Backbone motions in a crystalline protein from field-dependent H-2-NMR relaxation and line-shape analysis. Biopolymers 53:9–18
Maricq MM, Waugh JS (1979) NMR in rotating solids. J Chem Phys 70:3300–3316
Martinez JC, Pisabarro T, Serrano L (1998) Obligatory steps in protein folding and the conformational diversity of the transition state. Nat Struct Biol 5:721–729
Palmer-III AG, Williams J, McDermott AE (1996) Nuclear magnetic resonance studies of biopolymer dynamics. J Phys Chem 100:13293–13310
Pauli J, Van Rossum B-J, Förster H, De Groot HJM, Oschkinat H (2000) Sample optimization and identification of signal patterns of amino acid side chains in 2D-RFDR spectra of the a-spectrin SH3 domain. J Magn Reson 143:411–416
Redfield AG (1957) On the theory of relaxation processes. IBM J Res Dev 1:19–31
Reif B, Griffin RG (2003) ^{1}H detected ^{1}H, ^{15}N correlation spectroscopy in rotating solids. J Magn Reson 160:78–83
Reif B, Jaroniec CP, Rienstra CM, Hohwy M, Griffin RG (2001) ^{1}H–^{1}H MAS correlation spectroscopy and distance measurements in a deuterated peptide. J Magn Reson 151:320–327

Reif B, Xue Y, Agarwal V, Pavlova MS, Hologne M, Diehl A, Ryabov YE, Skrynnikov NR (2006) Protein side-chain dynamics observed by solution- and solid-state NMR: comparative analysis of methyl ^{2}H relaxation data. J Am Chem Soc 128:12354–12355

Sackewitz M, Scheidt HA, Lodderstedt G, Schierhorn A, Schwarz E, Huster D (2008) Structural and dynamical characterization of fibrils from a disease-associated alanine expansion domain using proteolysis and solid-state NMR spectroscopy. J Am Chem Soc 130:7172–7173

Skrynnikov NR (2007) Asymmetric doublets in MAS NMR: coherent and incoherent mechanisms. Magn Res Chem 45:S161–S173

Tjandra N, Szabo A, Bax A (1996) Protein backbone dynamics and ^{15}N chemical shift anisotropy from quantitative measurement of relaxation interference effects. J Am Chem Soc 118:6986–6991

Torchia DA, Szabo A (1982) Spin-lattice relaxation in solids. J Magn Reson 49:107–121

Vallurupalli P, Hansen DF, Kay LE (2008) Structures of invisible, excited protein states by relaxation dispersion NMR spectroscopy. Proc Natl Acad Sci USA 105:11766–11771

Wasmer C, Lange A, Van Melckebeke H, Siemer AB, Riek R, Meier BH (2008) Amyloid fibrils of the HET-s(218–289) prion form a beta solenoid with a triangular hydrophobic core. Science 319:1523–1526

Williams JC, McDermott AE (1995) Dynamics of the flexible loop of triosephosphate isomerase—the loop motion is not ligand-gated. Biochemistry 34:8309–8319

Wu XL, Zilm KW (1993) Cross-polarization with high-speed magic-angle spinning. J Magn Reson A 104:154–165

Wylie BJ, Franks WT, Rienstra CM (2006) Determinations of N-15 chemical shift anisotropy magnitudes in a uniformly N-15, C-13-labeled microcrystalline protein by three-dimensional magic-angle spinning nuclear magnetic resonance spectroscopy. J Phys Chem B 110:10926–10936

Wylie BJ, Sperling LJ, Frericks HL, Shah GJ, Franks WT, Rienstra CM (2007) Chemical-shift anisotropy measurements of amide and carbonyl resonances in a microcrystalline protein with slow magic-angle spinning NMR spectroscopy. J Am Chem Soc 129:5318–5319

Xu J, Xue Y, Skrynnikov NR (2009) Detection of nanosecond time scale side-chain jumps in water/glycerol solvent. J Biomol NMR (in press) (topical issue on dynamics)

Yao L, Vögeli B, Ying J, Bax A (2008) NMR determination of amide N–H equilibrium bond length from concerted dipolar coupling measurements. J Am Chem Soc 130:16518–16520

Zeeb M, Jacob MH, Schindler T, Balbach J (2003) N-15 relaxation study of the cold shock protein CspB at various solvent viscosities. J Biomol NMR 27:221–234

Zhang Q, Sun XY, Watt ED, Al-Hashimi HM (2006) Resolving the motional modes that code for RNA adaptation. Science 311:653–656